Deformation associated with the 1997 eruption of Okmok volcano, Alaska

Dörte Mann and Jeffrey Freymueller
Geophysical Institute, University of Alaska, Fairbanks, Alaska, USA

Zhong Lu
Raytheon ITSS, USGS/EROS Data Center, Sioux Falls, South Dakota, USA

Received 16 January 2001; revised 5 September 2001; accepted 27 September 2001; published 17 April 2002.

[1] Okmok volcano, located on Umnak Island in the Aleutian chain, Alaska, is the most eruptive caldera system in North America in historic time. Its most recent eruption occurred in 1997. Synthetic aperture radar interferometry shows deflation of the caldera center of up to 140 cm during this time, preceded and followed by inflation of smaller magnitude. The main part of the observed deformation can be modeled using a pressure point source model. The inferred source is located between 2.5 and 5.0 km beneath the approximate center of the caldera and ~5 km from the eruptive vent. We interpret it as a central magma reservoir. The preeruptive period features inflation accompanied by shallow localized subsidence between the caldera center and the vent. We hypothesize that this is caused by hydrothermal activity or that magma moved away from the central chamber and toward the later vent. Since all historic eruptions at Okmok have originated from the same cone, this feature may be a precursor that indicates an upcoming eruption. The erupted magma volume is ~9 times the volume that can be accounted for by the observed preeruptive inflation. This indicates a much longer inflation interval than we were able to observe. The observation that reinflation started shortly after the eruption suggests that inflation spans the whole time interval between eruptions. Extrapolation of the average subsurface volume change rate is in good agreement with the long-term eruption frequency and eruption volumes of Okmok. *INDEX TERMS:* 8419 Volcanology: Eruption monitoring (7280); 8434 Volcanology: Magma migration; 3210 Mathematical Geophysics: Modeling; *KEYWORDS:* Aleutian Arc, volcano deformation, InSAR, caldera activity

1. Introduction

[2] Okmok volcano is a basaltic shield with a 10-km-wide caldera at its summit that occupies most of the northeastern end of Umnak Island in the central Aleutians, Alaska (Figure 1). Two caldera-forming events occurred about 8000 and 2400 years ago [*Byers*, 1959]. Several major eruptions and a number of minor events have occurred in historic time, including 12 reported eruptions in the last century. The historic eruptive pattern suggests almost evenly spaced phases of activity that consist of a major event and preactivity or postactivity within 3 years [*Miller et al.*, 1998].

[3] The latest eruption of Okmok volcano began on 11 February 1997 when a steam and possible ash plume was reported, and it lasted for ~2 months [*Dean et al.*, 1998]. The eruption was a moderate Strombolian type with an ash plume reaching a height of up to 10 km and produced a basaltic lava flow covering an area of ~7.5 km^2. Like all historic eruptions of Okmok, the 1997 eruption originated from Cone A, located in the southern part of the caldera (Figure 1c).

[4] Okmok is a very active system that has generated repeated caldera-forming eruptions in the past and may do so in the future. Its eruption plumes are also a potential hazard for the heavy air traffic over the Aleutians. Crustal deformation measurements are useful to learn more about its magmatic system and eruptive behavior. Such measurements could help to recognize and interpret even subtle eruption precursors and may also give a better understanding of the way active caldera systems behave. However, Umnak Island, like most places in the Aleutians, is a very remote spot. Synthetic aperture radar (SAR) interferometry (InSAR) therefore can make a critical contribution to volcano monitoring and possible eruption forecasting in an area where there are no other geophysical instruments or data. A detailed description of the radar observations, coherence studies, and discussion of atmospheric delay anomalies is given by *Lu et al.* [2000]. In this paper we present the results of extensive deformation modeling and discuss the volcanological implications for Okmok.

0148-0227/02/2001JB000163$09.00

2. Observations

2.1. SAR Images and Interferograms

[5] The SAR data used in this paper, together with the relevant parameters for the interferograms formed from these images, are summarized in Table 1. All interferograms were corrected for topographic effects using a digital elevation model (DEM) derived from the U.S. Geological Survey (USGS) DEM and an interferogram using the ERS-1/2 tandem mission in 1995. The details of the SAR processing and interferogram derivation are given by *Lu et al.* [2000], along with a detailed analysis of the errors and preliminary deformation results. The figures shown here are enlargements of sections of the interferograms from *Lu et al.* [2000].

2.2. Deformation Episodes

[6] The observations span the time from 1992 to 1998. We distinguish three distinct phases in the time history of deformation: (1) preeruptive inflation and lateral magma transport (1992–1995), (2) coeruptive deflation (1995–1997), and (3) posteruptive inflation (1997–1998). Even though the eruption lasted only ~2

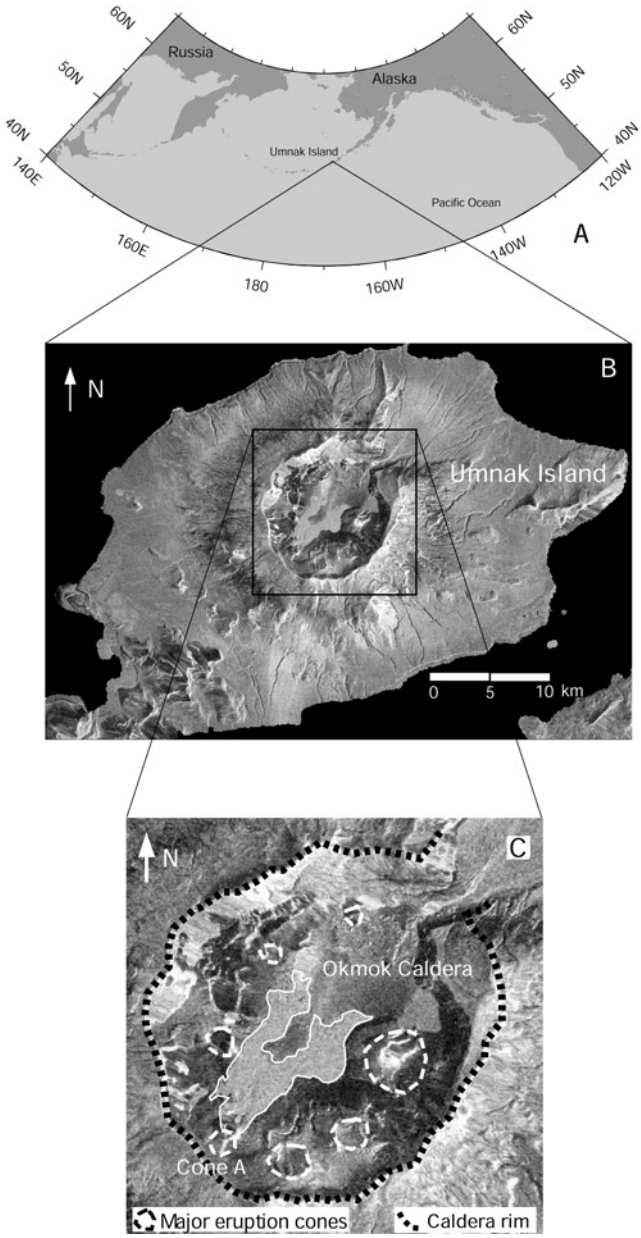

Figure 1. (a) Location of Umnak Island in the central Aleutian Arc, Alaska. (b) SAR image of the northern part of Umnak Island with Okmok caldera in the center. This image was acquired on 3 April 1997 shortly after the eruption had ceased. (c) Blowup of Okmok caldera. Outlined are cones of postcaldera activity, including Cone A, the vent site of the 1997 eruption, and the new lava flow.

months, we have to assign a 2-year-long coeruptive interval because no suitable SAR images were acquired between 1995 and 1997. For simplicity of description, in this section we describe the deformation as if it was entirely vertical. Our numerical models, however, take into account that the average look angle of the radar beam is 23° off the vertical and model the deformation projected into the line of sight direction, which includes a component of horizontal motion. The interferograms are shown with wrapped phases, ranging from 0 to 2π. One complete cycle represents 2.8 cm of relative motion. An increasing phase indicates relative motion away from the satellite (subsidence), while a decreasing phase indicates relative motion toward the satellite (uplift).

2.2.1. Preeruptive inflation and lateral magma transport (1992–1995). [7] From November 1992 to October 1993 we observe more than four fringes corresponding to at least 12 cm uplift of the center of the caldera (Figure 2a). The area of coherence is very limited, and it is likely that deformation extends beyond the visible fringes. Between November 1993 and October 1995, the fringe pattern is more complicated (Figure 3a): about two fringes indicate uplift around the same center as in the previous period. In addition, two centers of subsidence appear in the southwest of the caldera. Phase coherence in these interferograms is limited to patches within the caldera and more extensive areas outside the caldera. No significant deformation is observed outside the caldera [*Lu et al.*, 2000, Plates 3 and 5].

2.2.2. Coeruptive deflation (1995–1997). [8] From October 1995 to September 1997, about 50 fringes, corresponding to 140 cm of deflation, are visible around the caldera center. The deformation extends well beyond the caldera rim, with different fringe densities in different directions (Figure 4a). The newly erupted lava flow has changed the ground properties in the southern part of the caldera and causes a loss of coherence between the two acquisitions making up this interferogram. Coherence analysis has been used to map the extension of the flow and is a very accurate mapping tool in areas with otherwise good coherence [*Lu et al.*, 2000].

2.2.3. Posteruptive inflation (1997–1998). [9] During the year after the eruption, from September 1997 to September 1998, about three fringes, corresponding to 9 cm of uplift, are observed within the caldera (Figure 5a). The area of low coherence in the interferogram corresponds mostly to the region covered by the new lava erupted during February–April 1997. Along the edge of the flow, localized deformation is visible (Figure 6a and 6b. This deformation is relative uplift centered in the area between the two arms of the flow (Figure 6c). Outside the caldera, coherence is well maintained, but no significant deformation is observed [*Lu et al.*, 2000, Plate 8]. However, the coherent areas inside and outside the caldera cannot be connected.

3. Modeling

[10] We modeled the observed deformation using spherical pressure sources [*Mogi*, 1958] and a rectangular dislocation source [*Okada*, 1985] in an elastic half-space. Using a dense grid search,

Table 1. Satellite Data Used in This Study[a]

Orbit Image 1[b]	Acquisition Date	Orbit Image 2	Acquisition Date	h_a,[c] m	Figure
E1_06773	31 Oct. 1992	E1_12284	20 Nov. 1993	−568	2
E1_12012	1 Nov. 1993	E1_22376	25 Oct. 1995	−138	3
E1_22147	9 Oct. 1995	E2_12494	9 Sept. 1997	−695	4
E2_12723	25 Sept. 1997	E2_17733	10 Sept. 1998	108	5, 6
E1_11282	11 Sept. 1993	E1_22147	9 Oct. 1995	−103	

[a] For original interferograms, see *Lu et al.* [2000].
[b] E1 and E2 denote ERS-1 and ERS-2 satellites, respectively.
[c] The parameter h_a is the altitude of ambiguity.

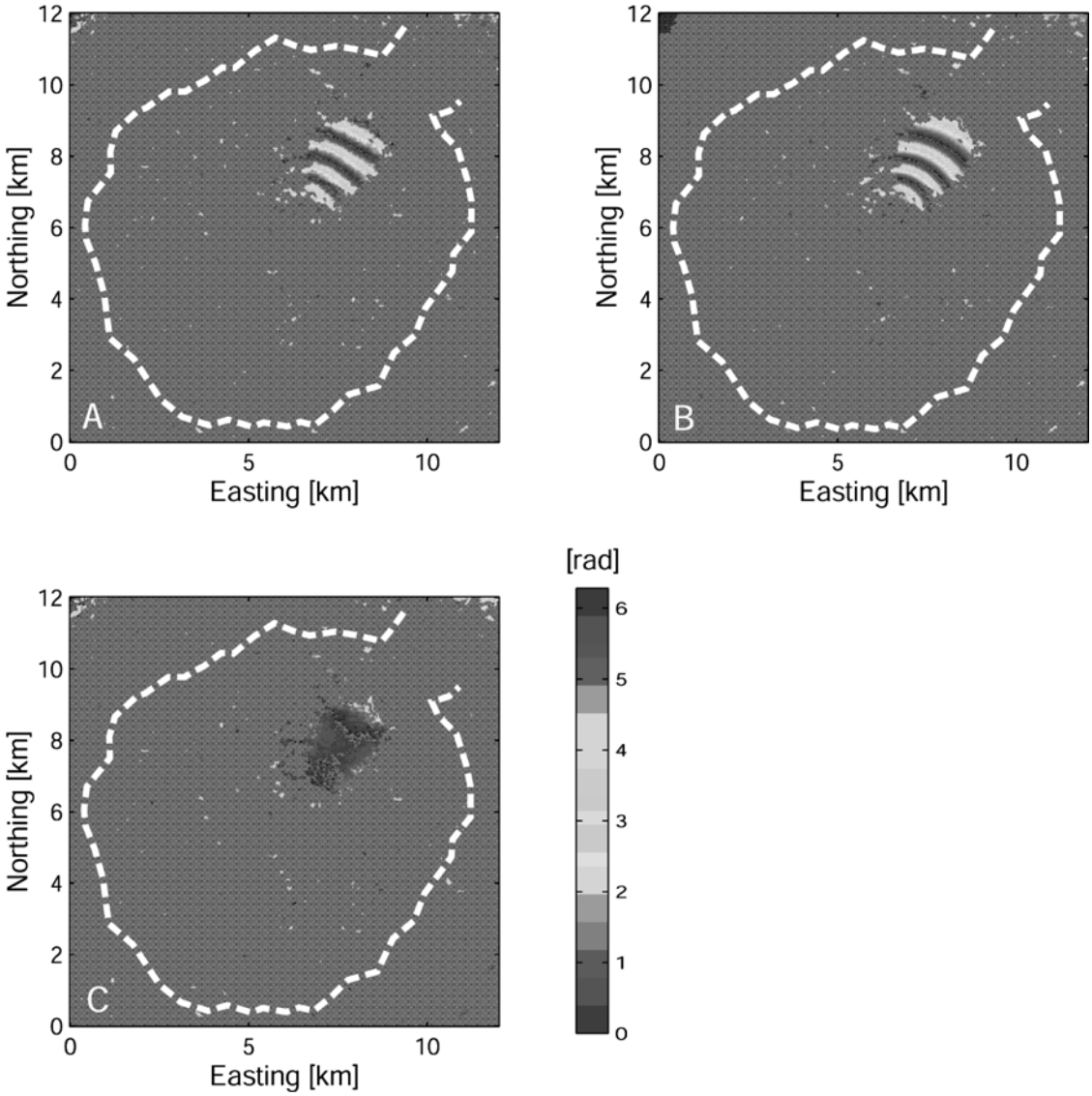

Figure 2. (a) Data, (b) best fit model, and (c) residual interferogram for the 1992–1993 preeruptive interferogram. The dashed line outlines the caldera. The origin of the coordinate systems is at 53.377°N, 168.220°W. See color version of this figure at back of this issue.

we derived the model parameters that give the best fit to the data in a least squares sense for each interferogram.

3.1. The Models

[11] The parameters for the Mogi model are horizontal source coordinates, source depth, and source strength. The observed deformation at the surface is given by

$$\Delta h(r) = Cd/\left(r^2 + d^2\right)^{3/2} \quad (1)$$

$$\Delta r(r) = Cr/\left(r^2 + d^2\right)^{3/2}, \quad (2)$$

where Δh and Δr are the vertical and horizontal (radial) displacements, C is the source strength, d is the source depth, and r is the distance from the source. The Mogi source is commonly interpreted as a magma chamber, and the source strength contains an inseparable combination of chamber size, pressure change, and elastic parameters, $C = 3a^3\Delta P/4\mu$, with source radius a, pressure change ΔP, and Lamé constant μ. The point source approximation is only valid if the dimension of the source (radius a) is much smaller than its depth d. Especially for the very shallow subsidence structures in the 1993–1995 interferogram this assumption may be violated.

[12] Rectangular dislocation sources are used to simulate emplacement of dikes or sills. The parameters for the rectangular dislocation model are length, width, strike, dip, and geographical location of the dislocation plane, as well as dip-slip, strike-slip, and opening dislocations. For a simple dike model we constrain dip-slip and strike-slip to be zero in our modeling.

3.2. Data Selection and Procedures

[13] In each interferogram we selected areas with phase coherence above a specified threshold (see unmasked areas in Figures 2–5). We then selected simple polygonal regions of connected pixels from these coherent areas for input to the modeling algorithm. This approach allowed us to select the usable data without having to deal with many small, unconnected regions of coherence (see Figure 2 for an example).

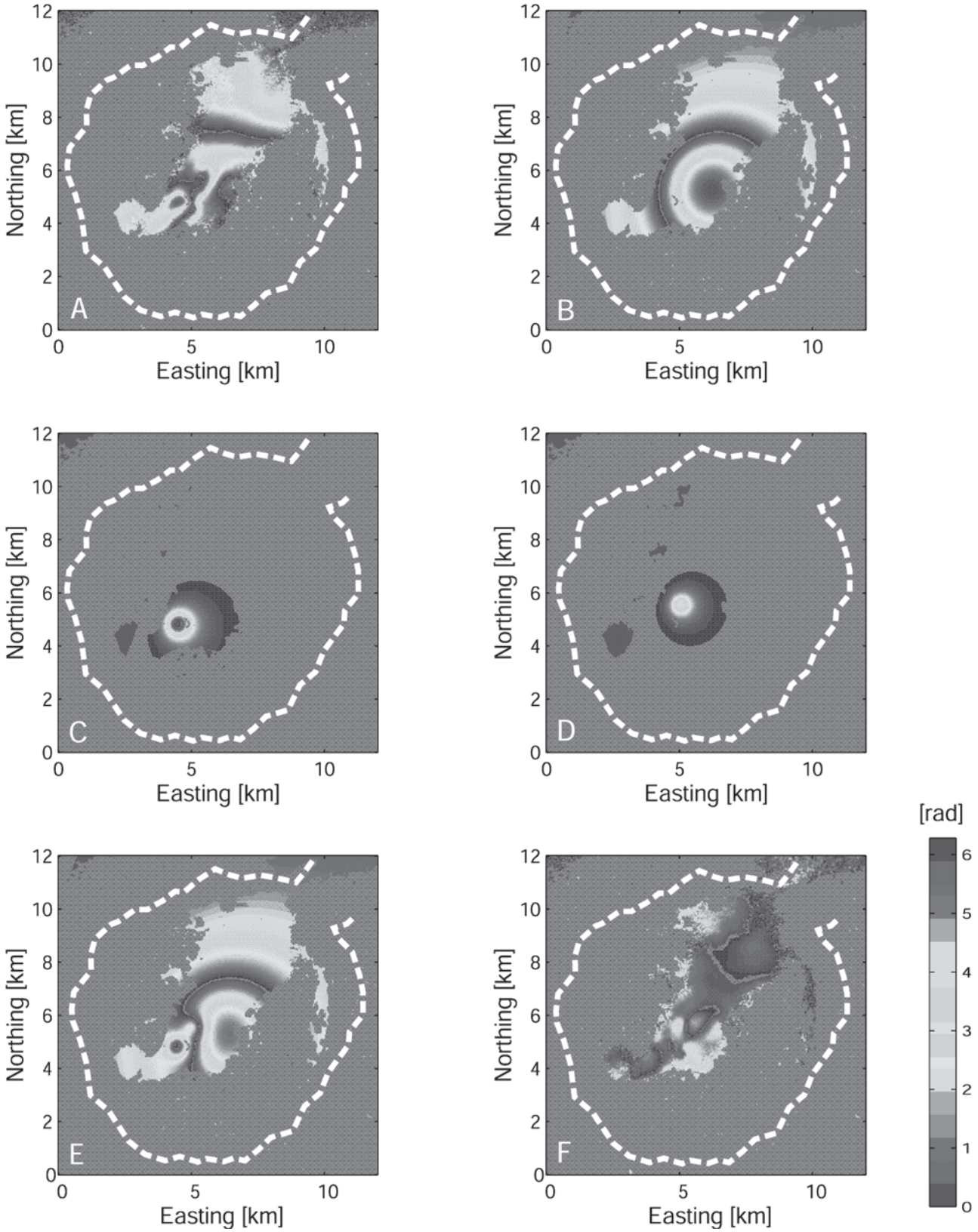

Figure 3. (a) Data, (e) best fit model, and (f) residual interferogram for the 1993–1995 preeruptive interferogram. (b, c, d) The model, consisting of three point sources with different depths and strengths. Annotations and origin of coordinate system are the same as in Figure 2. See color version of this figure at back of this issue.

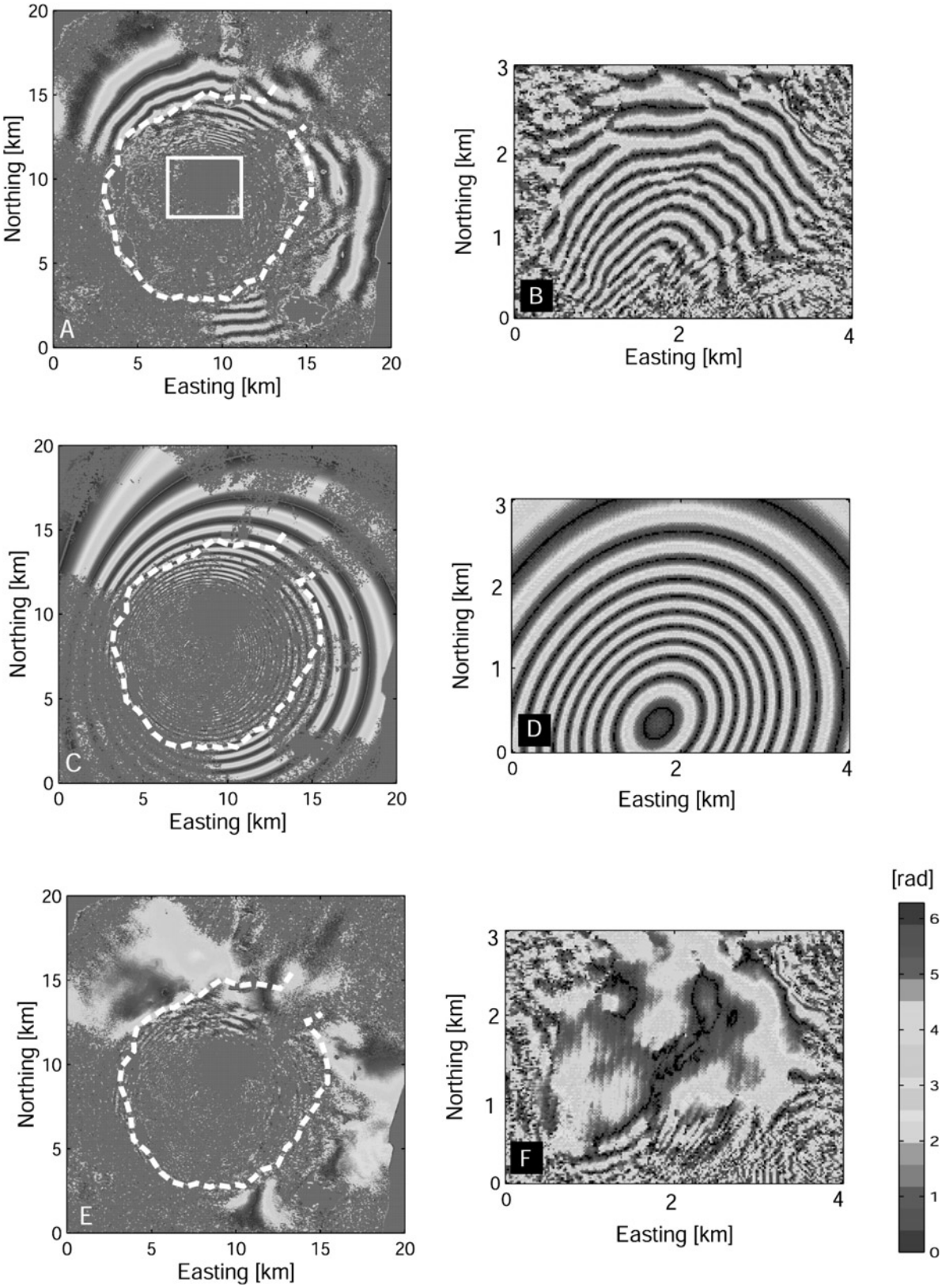

Figure 4. Data, models, and residuals for the 1995–1997 coeruptive interferogram. (a) Data of the 1995–1997 interferogram. The box outlines the area shown in Figures 4b, 4d, and 4f. The fringe density in the caldera center is too high to be properly displayed in Figure 4a. (b) Blowup of the data inside the caldera after subtracting the fringes explained by the best fit Mogi model for the outer part of the deformation shown in Figure 4c. (d) Best fit rectangular dislocation source for this data inside the caldera. (e) Residual interferogram for the combined modeling. (f) A blowup of the same residual interferogram, showing the model fit inside the caldera. The origin of the coordinate system for the large area is at 53.357°N, 168.257°W. See color version of this figure at back of this issue.

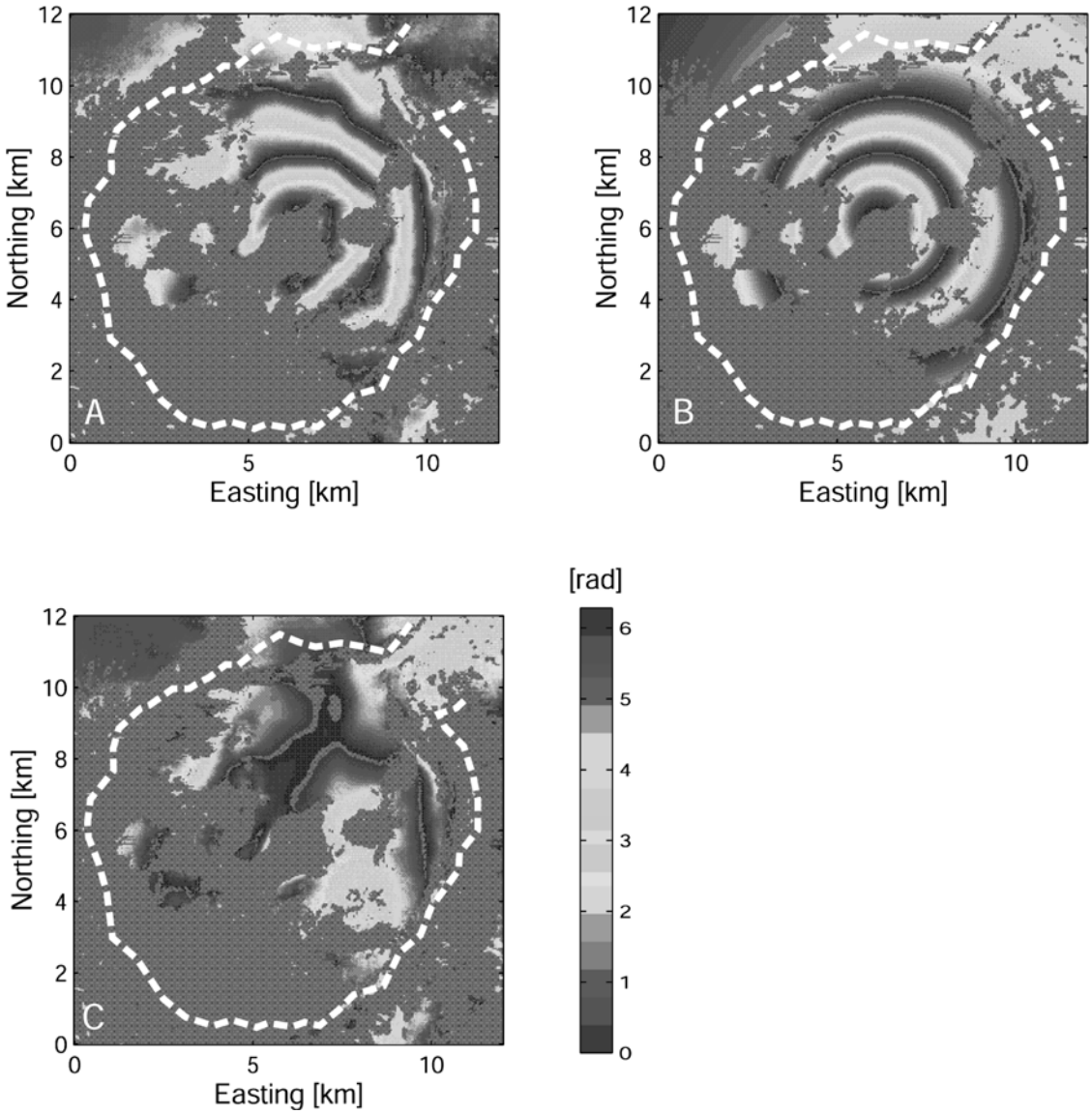

Figure 5. (a) Data, (b) best fit model, and (c) residual interferogram for the 1997–1998 posteruptive interferogram. Annotations and origin of coordinate system are the same as in Figure 2. See color version of this figure at back of this issue.

[14] The best fit model for an interferogram is based on the best fit in these areas in a least squares sense. We generally modeled the wrapped data. This avoids introduction of errors caused by the unwrapping algorithm, especially in areas where the fringe density is very high, e.g., inside the caldera in the 1995–1997 interferogram (Figure 4a). Doing this, one has to be careful though to eliminate ambiguities caused by the periodicity of the signal. However, the model can be checked by comparing the total number of fringes in the data in the modeled interferogram.

3.3. Misfit Calculation for Wrapped Interferograms

[15] The general model equations for a wrapped interferogram reflects the fact that all phase values are modulo 2π and is given by

$$\mathrm{mod}(\phi, 2\pi) = \mathrm{mod}[\boldsymbol{G}(\boldsymbol{m}) + \xi + \varepsilon + 2\pi], \tag{3}$$

where ϕ is the vector of phase values, $\boldsymbol{G}(\boldsymbol{m})$ is the geophysical model for the deformation in terms of model parameters $\boldsymbol{m}$, ξ is an estimated bias parameter because the zero phase value is arbitrary, and ε is the vector of errors. For unwrapped interferograms the modulo functions would be removed. Equation (3) cannot be solved by standard least squares, even for a linear model, because the entire right-hand side is contained within the modulo function, which is nonlinear. However, an optimal solution to (3) can be found by grid search or Monte Carlo methods as long as a satisfactory misfit function is used. We define the misfit between the observed and synthetic phase to be the smallest angle between the two values, disregarding the branch cut at $0|2\pi$. This definition recognizes that the phase value ϕ_i may be interpreted equally well as ϕ_i or $\phi_i + 2n\pi$. Thus the misfit of a given model to the data is given by the square root of the sum of squares (RSS) of the residuals with

$$\mathrm{RSS} = \sum \epsilon_i^2; \quad \epsilon_i = \min(\phi_i - c_i, \ \phi_i + 2\pi - c_i)$$
$$c_i = \mathrm{mod}\left[\boldsymbol{G}(\boldsymbol{m})_i + \xi_i, 2\pi\right]. \tag{4}$$

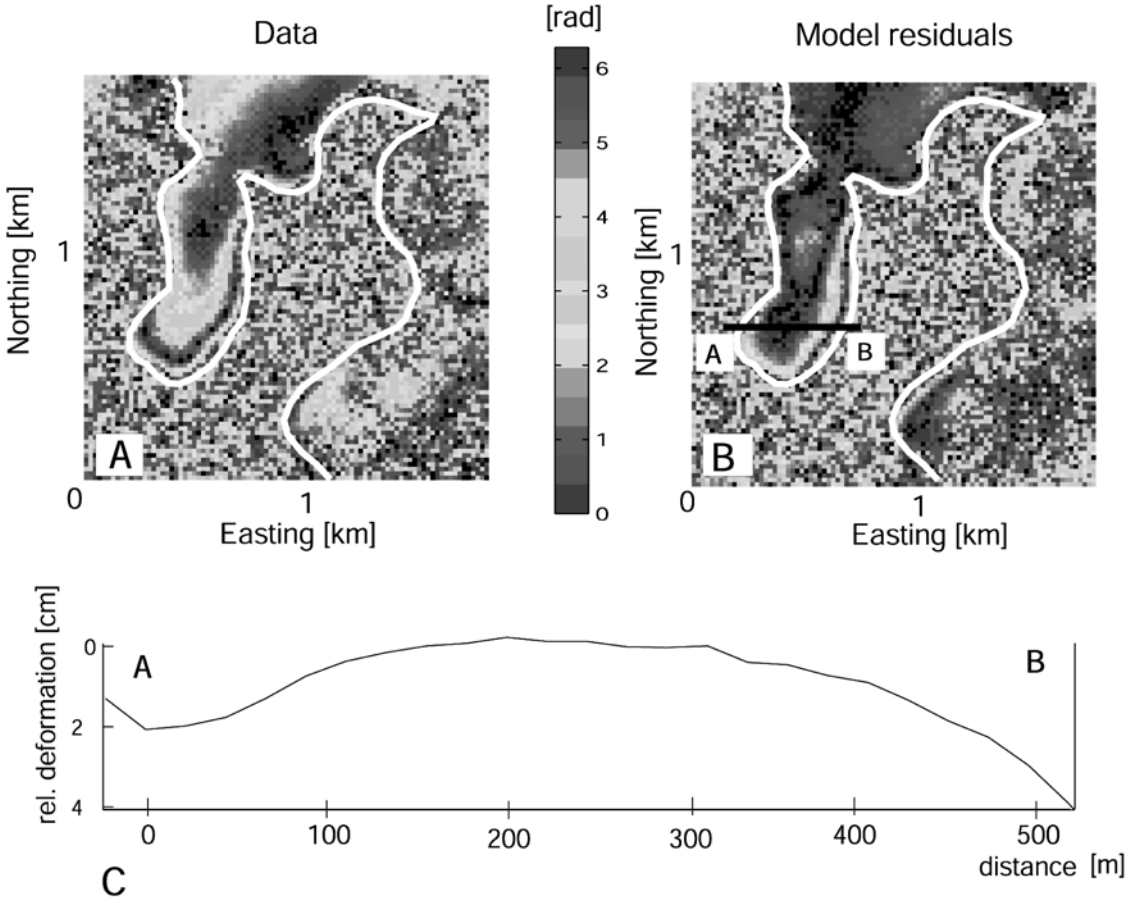

Figure 6. (a) Deformation fringes along the edges of the new lava flow as observed in the 1997–1998 interferogram. The white line outlines the flow boundary. (b) Residual fringes along the edge of the flow after subtracting the best fit Mogi inflation model from the data. The black line marks the profile shown in Figure 6c. (c) Deformation profile as marked in Figure 6b. Relative deformation across the profile is ~3 cm. See color version of this figure at back of this issue.

4. Subsurface Volume Change, Magma Volume, and Pressure Change

[16] In the Mogi model the observed surface deformation can be caused by different subsurface processes, primarily by pressure change, volume change, or a combination of both. In terms of processes in magma chambers, this gives us a variety of interpretations for the observed inflation or deflation signal. In the case of inflation we can distinguish the following end-members: volume increase of the reservoir due to influx of new magma, and internal pressure increase of the magma already present in the reservoir, with no change in mass. In the case of deflation the subsurface volume change can likewise be due to withdrawal of magma, either erupting at the surface or migrating to a different place, or internal magma pressure decrease.

[17] New magma rising from a deeper level by means of buoyancy adds volume to an existing reservoir. Treating magma as an incompressible fluid, the subsurface volume change would be equal to the volume of new magma. For this case, *Delaney and McTigue* [1994] derive

$$\Delta V_{\text{subsurface}} = \frac{\pi u_z^{\max} d^2}{(1-\nu)}, \tag{5}$$

where $u_z^{\max}$ is the maximum vertical surface displacement, d is the source depth, and ν is the Poisson ratio of the host rock. In terms of source strength C, (5) can be written as

$$\Delta V_{\text{subsurface}} = \frac{4}{3}\pi C. \tag{6}$$

At the other extreme, an internal pressure increase can result from fractional crystallization of nonhydrous components and the resulting oversaturation of the melt with volatiles [*Tait et al.*, 1989]. This pressure increase eventually leads to expansion of the system

$$\Delta V_{\text{subsurface}} = \pi \frac{\Delta P}{\mu} a^3, \tag{7}$$

where ΔP is the pressure change, a is the source radius, and μ is the rigidity of the surrounding rock. Equation (7) is actually just a different form of (6); in other words, the two mechanisms are indistinguishable based on deformation measurements alone.

[18] Equations (6) and (7) allow us to estimate the upper bounds of pressure and volume changes due to the single processes. A quantitative analysis of the pressure change requires the additional knowledge about the size of the magma reservoir and elastic

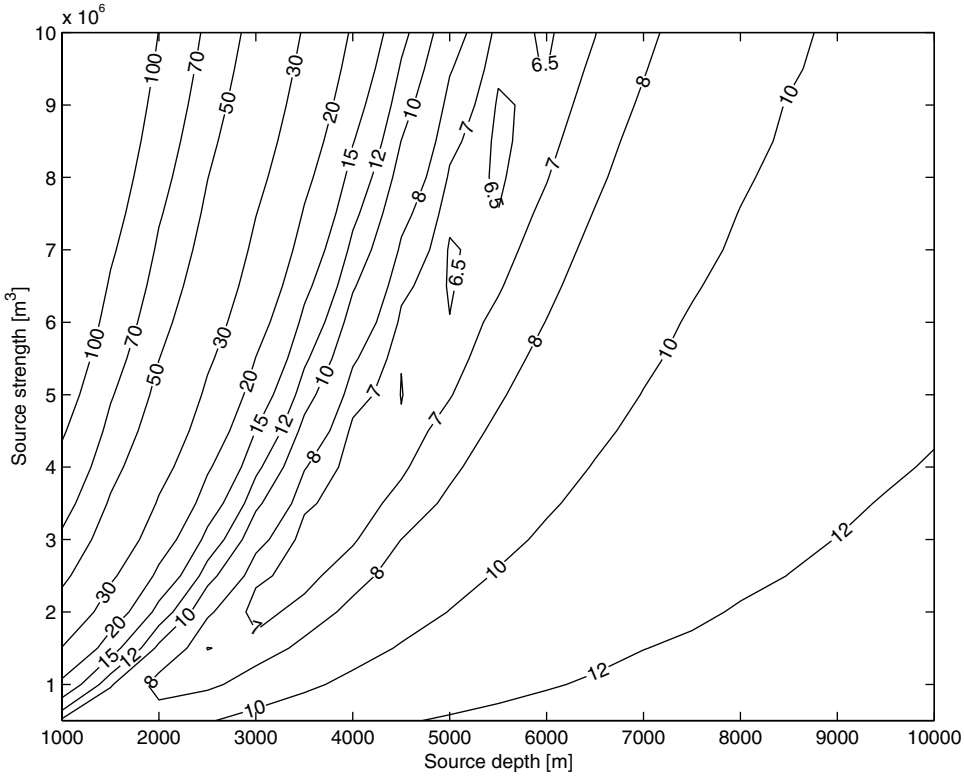

Figure 7. Contour plot of the RMS error (in radians) for an unwrapped interferogram, showing the trade-off between source depth and strength, here for the model of the 1992–1993 interferogram.

parameters. In practice, deformation will most likely be due to a combination of both processes.

[19] It is possible to trigger an eruption just by internal pressure increase [*Tait et al.*, 1989] causing inflation, but a magma surplus must accumulate before or during the eruption for a significant volume to be erupted. An eruption will eventually stop when the overpressure in the magma chamber is released by explosive activity and/or extrusion of lava. This means that both pressure and magma volume have decreased. The remaining magma will expand in the chamber due to the pressure release and diminish the observed volume loss. An internal pressure decrease has the contrary effect and leads to overestimation of the magma volume erupted or moved.

[20] If explosivity is low and a significant amount of lava is extruded, which is the case for Okmok, it is very likely that magma intrusion, extrusion, and movement are the main factors causing the observed deformation. For volume calculations at Okmok we will assume that the pressure changes were not significant relative to the volume changes. The suitability of this assumption can be debated, but we have no data that independently determine pressure or volume changes.

5. Modeling Results and Interpretation

5.1. Preeruptive Inflation and Lateral Magma Transport (1992–1995)

[21] The 1-year interferogram spanning the time from October 1992 to November 1993 can be modeled as pure inflation (Figures 2b and 2b). The horizontal location of the source is well-constrained on the basis of the shape of the fringes. It is difficult to constrain the depth because coherent data inside the caldera are very limited and adjustment of the source strength gives a range of equally fitting depths. Using the data inside the caldera, we find suitable models with a source depth ranging from 2.5 to 6.5 km (Figure 7). We have means to constrain the maximum depth somewhat better by looking at the coherent areas outside the caldera. Ten kilometers away from the caldera center, we find coherent areas that show no more than a fraction of a fringe [see *Lu et al.*, 2000, Plate 3], which allows us to rule out a strong, deep source. Most of the small phase variations outside the caldera are due to atmospheric effects [*Lu et al.*, 2000]. With the assumption of a maximum relative deformation of 0.014 m (half a fringe) between 10 and 15 km distance from the center of deformation, we determine a maximum source depth of 4.1 km. If we limit the maximum deformation to 0.009 m (one third of a fringe), the maximum source depth would be 3.6 km (Figure 8). For depths from 2.5 to 4.1 km the corresponding source strength ranges from 9.5×10^5 m^3 to 3.5×10^6 m^3. Using relation (6), this corresponds to a subsurface volume change of $+4 \times 10^6$ m^3 to $+15 \times 10^6$ m^3.

[22] The interferogram from November 1993 to October 1995 contains signals from multiple mechanisms (Figures 3b and 3c). First, there is continuing inflation located underneath the caldera center. It is significantly weaker than during the 1992–1993 period. The source is located between 2.5 and 5.1 km depth. We constrain the maximum depth by the same method used for the 1992–1993 interferogram, allowing in this case a maximum signal of half a fringe between 8 and 13 km distance from the deformation center (Figure 8). The inferred subsurface volume change for this inflation source is then between $+2 \times 10^6$ m^3 to $+9 \times 10^6$ m^3.

[23] In addition, there are two localized areas of subsidence. The best fit Mogi source for both of them is at 500 m depth, with volume changes of -2×10^4 m^3 and -4×10^4 m^3, respectively. They are located 0.7 and 1.4 km from the inflation source toward the southwest (Figure 9). The deformation from these sources is quite small, but an independent interferogram for the same time period (Table 1) shows the same features and confirms that they are crustal deformation and not atmospheric anomalies. We also tried to model part of the deformation in this interferogram as dike

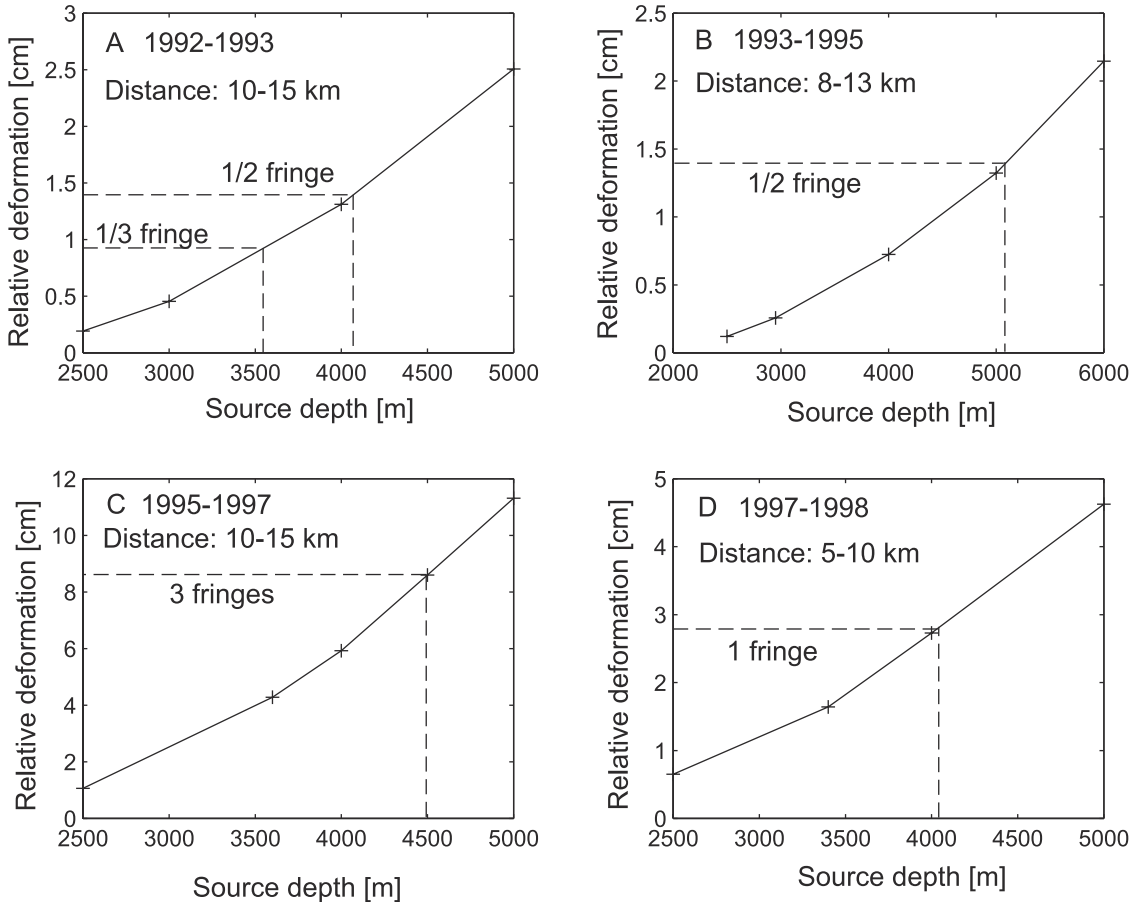

Figure 8. Predicted relative deformation outside the caldera as a function of source depth. The distances from the center of deformation depend on the existence of coherent areas. Therefore they are chosen for each interferogram individually. (a) From 1992 to 1993 interferogram, with at most half a deformation fringe detected between 10 and 15 km from the center. This constrains the source depth to 4.1 km. A third of a fringe translates into a depth of 3.6 km. (b) From 1993 to 1995, with a maximum of half a deformation fringe existing between 8 and 13 km from the center. This allows a maximum source depth of 5.1 km. (c) From 1995 to 1997, with a maximum of three fringes appearing between 10 and 15 km from the center, constraining the source depth to 4.5 km. (d) From 1997 to 1998, with at most one fringe existing between 5 and 10 km from the center, constraining the source depth to <4.1 km.

intrusion [*Okada*, 1985]. However, the data fit was considerably worse for a dike source than for Mogi sources. The areas where these two shallow sources are found lies outside the region of coherence in the 1992–1993 interferogram, so we cannot know if they were present before 1993.

5.2. Coeruptive Deflation (1995–1997)

[24] The fringe pattern of the interferogram from October 1995 to September 1997 is best modeled by a combination of a point deflation source and a closing rectangular dislocation source. The point source fits the deformation outside the caldera (Figures 4c and 4e). It is located at ~3.6 km depth, with a maximum depth of 4.5 km, estimated by the lateral extension of the deformation signal (Figure 8). This indicates a subsurface volume change of -5×10^7 m^3 to -9×10^7 m^3.

[25] Adding a rectangular dislocation source significantly improved the fit for the deformation inside the caldera (Figures 4d and 4f). Its parameters translate to a 2.5-km-long, 1.5-km-wide sill, located at 1.8 km depth. It is striking N50°E, and dipping 5° from the horizontal to the northwest. The upper southwest corner is located at 53.428°N and 168.136°W. This corresponds approximately to the center of deflation. The amount of closure is 0.9 m, giving an additional volume change of -3.4×10^6 m^3. Figures 4e and 4f show the residuals of the combined model.

5.3. Posteruptive Inflation (1997–1998)

[26] The concentric part of the deformation signal from September 1997 to September 1998 is modeled by a point source between 3.5 and 4.1 km depth, which is in the same range estimated for the preeruptive inflation source (Figures 5b and 5c). Because the center of deformation corresponds to an area with low coherence, minimum source depth and strength are relatively difficult to constrain. Coherent areas outside the caldera do not show deformation farther than 10 km away from the center of deformation which constrains the maximum source depth to 4.1 km (Figure 8). The inferred subsurface volume change is $+4 \times 10^6$ m^3 to $+8 \times 10^6$ m^3. The Mogi source explains the main deformation signal, but localized deformation immediately adjacent to the lava flow remains unmodeled.

[27] An additional interesting phenomenon is deformation along the edge of the new lava flow (Figure 6a). It shows uplift of the center area between the two arms of the overlying new lava flow relative to the edges of the flow. Because there is no absolute reference, it could also be interpreted as subsidence of the edges relative to the center. Because the new lava flow did not maintain

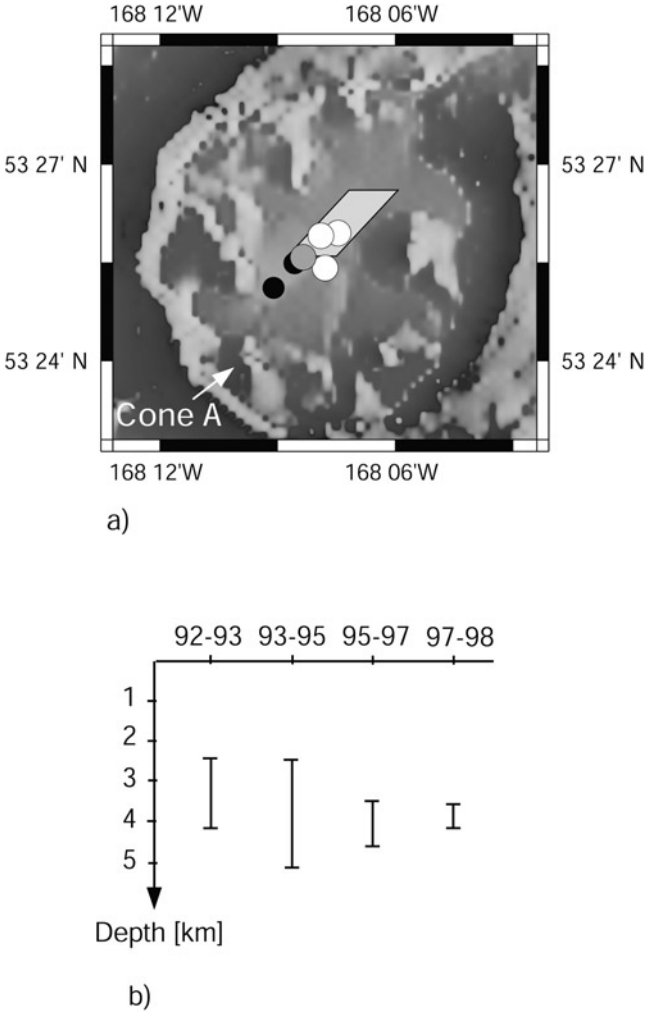

Figure 9. (a) Location of deformation sources for modeled episodes in map view. Shown are preeruptive and posteruptive inflation sources (open circles), the main coeruptive deflation source (shaded circle), areas of preeruptive subsidence (solid circles), and the coeruptive closing sill (shaded rectangle). (b) Vertical locations for Mogi sources for modeled episodes. Depths range from 2.5 to 5.1 km, but uncertainties are too large to recognize a trend.

coherence during this time interval, we do not know if it is also affected by the same sense of deformation. Possible explanations for the cause of this deformation are (1) elastic or viscoelastic deformation caused by the load of the new flow, (2) heating and thereby deforming of an underlying older flow after extrusion of the new flow, and (3) mechanical destruction and compaction of this older flow.

[28] Simple calculation of thermal deformation of volcanic products shows that in general, heating can be ruled out as a cause for this deformation. Mechanical destruction of the rough and blocky surface of the old flow by the overriding 1997 flow would probably lead to loss of coherence which would destroy the signal itself. Also, it should happen during or right after the new flow is emplaced. However, we observe the deformation between September 1997 and September 1998, i.e., starting at least about half a year after all the lava had been extruded.

[29] *Briole et al.* [1997] used a model of substrate relaxation in response to loading to explain a similar phenomenon observed at Etna volcano. We propose that the same mechanism causes deformation adjacent to the 1997 flow of Okmok, superimposed on the ongoing inflation of the caldera floor. After subtracting the signal due to inflation from the data, 2–4 cm of relative deformation remain (Figures 6b and 6c). The fact that the deformation extends ~150 m away from the outer edge of the new flow (Figures 6a and 6b) makes an explanation by heating and mechanical destruction/compaction of the older flow unlikely. Relaxation due to loading however extends well beyond the edge of the flow [*Briole et al.*, 1997].

5.4. Summary

[30] Despite its simplicity, the Mogi model can explain most of the deformation related to Okmok's 1997 eruption very well, except for parts of the deflation that occurred between 1995 and 1997. Best fitting model parameters for all Mogi sources are listed in Table 2. Horizontal and vertical locations of all estimated source models are also summarized in Figure 9. The source depth ranges between 2.5 and 5.1 km, but uncertainties are too large to be confident that this difference is significant. The horizontal source location is better constrained. All inflation sources and the main deflation source are located beneath the caldera center, within an area a kilometer across. The subsidence structures observed between 1993 and 1995 (solid circles in Figure 9) are located southwest of the caldera center on an almost straight line toward Cone A, the later eruptive vent. The modeled sill in the 1995–1997 interferogram extends from the deflation center during that period to the northeast. It is 2.5 km long, 1.5 km wide, and 0.9 m thick. It is located at 1.8 km depth and has a volume of 3.4×10^{-3} km^3. The fact that our best model for this interferogram consists of a combination of two different sources does not necessarily mean that we actually have two independent structures causing the deformation. It could also indicate a deviation from the point source geometry of the main source. The lack of data from the southwest part of the caldera (the area covered by the new lava flow) makes it difficult to determine the complexity of the source or the full extent of the sill.

6. Discussion

6.1. Temporal Development of Deformation and Magma Volume

[31] The sequence of preeruptive inflation, coeruptive deflation, and posteruptive inflation has been observed at many volcanoes (e.g., Etna [*Lanari et al.*, 1998]). It is usually explained with the

Table 2. Parameters for the Best Fit Mogi Source Model for All Deformation Episodes

Time Period	Depth, km	Strength, 10^{-3} km^3	Volume, 10^{-3} km^3	Latitude, °N	Longitude, °W
1992–1993	2.5–4.1	0.95–3.5	4.0–14.7	53.433	168.124
1993–1995	2.5–5.1	0.3–2.15	1.3–9.0	53.424	168.129
	0.5	−0.01	−0.44	53.419	168.151
	0.5	−0.005	−0.22	53.425	168.143
1995–1997	3.6–4.5	−12.50–(−21.95)	−52.4–(−91.9)	53.431	168.133
1997–1998	3.5–4.1	1.0–1.9	4.2–7.9	53.432	168.131

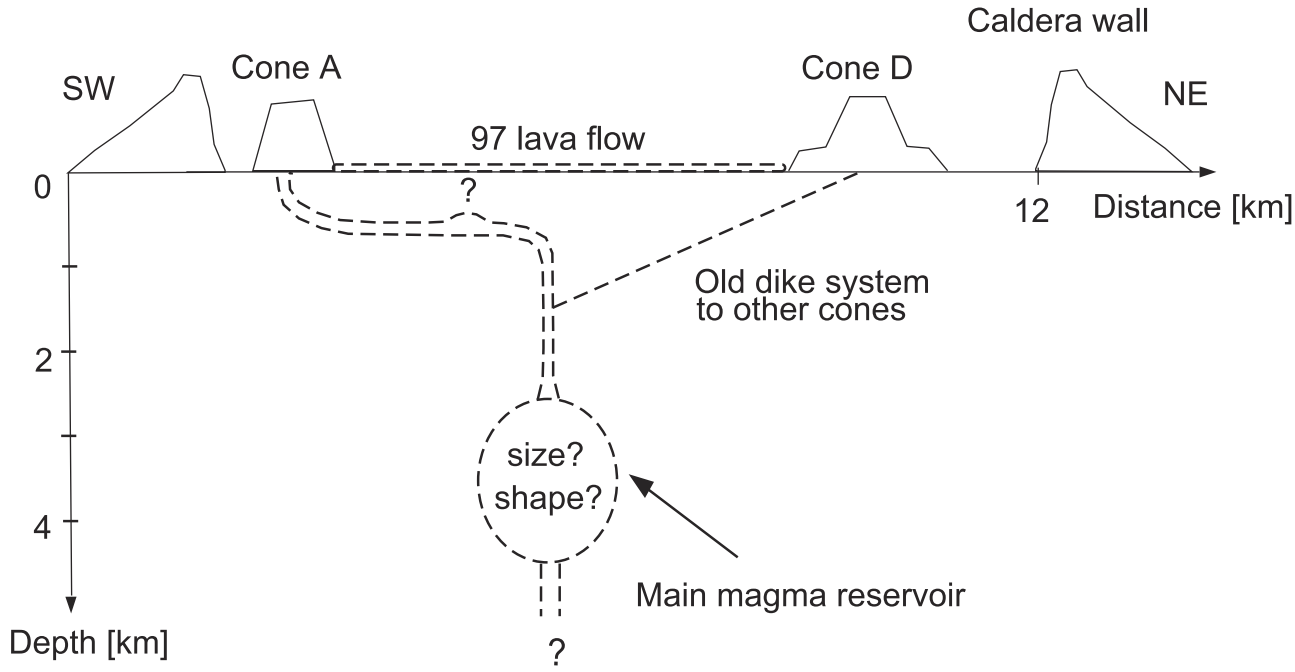

Figure 10. Structural model of Okmok volcano as interpreted from deformation modeling results. See text for detailed description.

periodic filling and emptying of the magma chamber. At Etna the posteruptive deformation source seems to be significantly deeper than the preeruptive source (12 km as opposed to 9 km). *Lanari et al.* [1998] explain this by refilling of the volcano system from below. Considering the difficulty in constraining the source depth, we do not see a similar change in source depths of this order during the inflation episodes at Okmok. During the coeruptive deflation period the best fitting model gives a somewhat deeper source depth. However, the high fringe density causes the model misfit to be larger here than in the other interferograms, and the difference may not be significant.

[32] The inflation rate during the preeruptive period is not constant. From 1993 to 1995 it is significantly smaller than between 1992 and 1993. This could either indicate a variation in the magma flux or be due to redistribution of magma in the shallow subsurface. The total 1992–1995 preeruptive inflation volume can account for only ~11% of the coeruptive deflation volume (up to 25% if we base our calculations on the maximum source depth for all models). We therefore infer that inflation must have been going on long before 1992. Since no InSAR data were acquired before that time and no other geodetic data exist from Okmok volcano, we cannot know how long Okmok has been inflating. Extrapolation of the average volume change rate of $\sim +2 \times 10^6$ m^3 yr^{-1} seen during the 1992–1995 period would require 28 years of inflation to account for the observed deflation. If we base our calculations solely on the 1992–1993 rate, which is twice as high, only 14 years are required. Okmok's last major lava-producing eruption of comparable size before 1997 occurred in 1958, 39 years ago. If reinflation starts directly after an eruption, as suggested by the current posteruptive observations, at some point Okmok's inflation rate has either been somewhat slower than observed in the last 3 years before the 1997 eruption or episodes of deflation have interrupted the cycle. The latter possibility is not unlikely because minor eruptive activity has been reported in 1960 and in the 1980s [*Miller et al.*, 1998]. We conclude that it is possible that Okmok is supplied with magma continuously, causing essentially continuous inflation. This is a similar situation as for Kilauea Volcano, Hawaii, which receives a steady supply of basalt magma, even though the source is different [*Delaney et al.*, 1990]. Future deformation observations with InSAR may allow us to determine more precisely the typical inflation rate for Okmok volcano and to correlate the state of inflation with type and timing of impending eruptions.

6.2. Lateral Magma Transport

[33] The center of maximum deformation for all episodes is offset ~5 km from Cone A, the eruptive vent. If we interpret the deflation source as Okmok's main magma chamber, then some sort of lateral magma transport is required to feed the eruption. There is a slight chance, of course, for an independent reservoir underneath Cone A. We do not have sufficient information in our data to rule this out, but we are confident that the sense of caldera floor motion (up before and after the eruption, down during the eruption) cannot be pure coincidence.

[34] We do not see an obvious dike intrusion in our data, but the temporal resolution of the data is only ~2 years during this period. More importantly, the 1995–1997 interferogram lacks coherence in the area where the effects of the dike would be seen due to the coverage of the old surface with new lava. This means we could easily have missed the signature of a dike intrusion. We do see some subsidence patterns in an overall inflation environment during 1993–1995. They may indicate withdrawal or movement of magma from some shallow body. In this case, magma must have been stored there before 1993 and withdrawn sometime between 1993 and 1995 to explain the observed subsidence. An alternative explanation is hydrothermal depressurization in that area, but with our data we have no means to distinguish between the two cases. Either way, these bodies may mark the pathway of magma from the central chamber to the eruptive vent.

[35] It is interesting to note that deformation was observed here at least 1.5–3.5 years before the start of the eruption. The signal of lateral transport may be a precursor that could distinguish between occasional deformation of calderas without eruptions (e.g., Yellowstone [*Wicks et al.*, 1998]) and deformation episodes that do lead to an eruption. The signal is subtle but well beyond noise, and

especially in the absence of other geophysical data it is a very valuable feature. We can exclude the possibility that it is just an anomaly caused by atmospheric delay because an independent interferogram spanning about the same time interval shows similar signals at exactly the same locations.

[36] There is no apparent structural reason why Cone A is the preferred intracaldera vent. Umnak Island and Okmok caldera are not subjected to major fault systems [*Nakamura et al.*, 1977]. The orientation of motion of the Pacific plate with respect to the North America plate is 325° [*DeMets et al.*, 1994]. This is roughly orthogonal to the direction of the presumed dike that transported magma from the caldera center to Cone A (220°). This suggests that the direction of the principal stress σ_1 beneath the volcano cannot be parallel to plate motion, so the local stresses generated by the magmatic system must be larger than the stresses generated by plate interaction. All postcaldera activity has been aligned along the periphery of the caldera floor, which indicates that ring fissures resulting from the caldera collapse are responsible for the location of the cones.

6.3. Proposed Structural Models

[37] Figure 10 summarizes schematically the interpretation of the modeled deformation in terms of volcanological structures. This interpretation does not claim to be a complete picture of the Okmok volcanic system since it is based mainly on one source of information, geodetic data. Instead, it is meant to serve as a basic working model that will be refined and modified with future acquisition of geological and geophysical data.

[38] From the closely spaced source locations for all main deformation episodes we conclude that Okmok has a central magma reservoir, located almost exactly at the geometric center of the caldera at 2.5–5.0 km depth. Considering the symmetry of the caldera, the same reservoir may have been responsible for the two caldera-forming eruptions as well as the postcaldera activity. Okmok appears to be characterized by a long-lived shallow magma chamber, which is filled quasi-continuously from a deeper source. Between eruptions, the caldera floor inflates due to magma accumulation in the central, shallow reservoir. The original depth of the magma source is not known. Petrological analysis of samples from recent lava flows and from rocks resulting from the two caldera forming events may give more insight into this problem in the future. This analysis may also help to determine if the hypothesis of a long-lived magma reservoir at a steady location is maintainable.

[39] Assuming a central chamber, the existence of six major cones concentrated on the periphery of the caldera indicates that the shallow subsurface is probably crossed by numerous dikes and fractures of varying orientation. This suggests that the local stress field has changed orientation through time. Up to a few years before an eruption, magma could move farther upward and spread out into this preexisting system of fractures, resulting in a lower surface inflation rate.

[40] During an eruption, magma is withdrawn from the reservoir and causes strong subsidence of the entire caldera floor. After the eruption the walls of the central magma chamber adjust to the new pressure conditions, and filling from the deeper source starts soon after. On the basis of the calculation of the slowest magma accumulation rate for Okmok, the filling process may actually continue at a constant rate throughout.

7. Conclusions

[41] The 1997 eruption of Okmok volcano was accompanied by significant deformation, expressed in particular by 140 cm of subsidence of the caldera floor during the eruption, and by preeruptive and posteruptive inflation of smaller amplitude centered at the same location. We interpret the deformation source as a magma reservoir at 2.5–5.0 km depth. The preeruptive inflation indicates magma influx into this reservoir and suggests ascent to a shallower level. In addition to the inflation, localized subsidence occurs ~0.7 km and 1.4 km from the caldera center, roughly one third of the way toward the later vent. This may be an indication of lateral magma movement as early as 2–3 years before the actual start of the eruption, or an expression of hydrothermal depressurization. The posteruptive inflation source is interpreted as pressure readjustment and/or refilling of the magma system beneath Okmok caldera. Okmok's eruptive history suggests that the average subsurface volume change rate shortly before the 1997 eruption is typical for the long term. In fact, Okmok may be supplied continuously from a deep source. Future observations at Okmok will enable us to learn more details about the typical deformation characteristics like duration, rate, and rate changes of preeruptive inflation and correlation to actual eruptions. This will be of great value not only for our knowledge about Okmok but also similar volcanoes and the magmatic processes in the Aleutian volcanic arc.

[42] **Acknowledgments.** We thank P. Briole, D. Dzurisin, and P. Lundgren for constructive comments on the manuscript. D. Mann, J. Freymueller, and Z. Lu were supported by NASA grant NAG5-4369. Lu was also supported by USGS contract 1434-CR-97-CN-40274. ERS-1 and ERS-2 SAR images are copyright 1992, 1993, 1995, 1997, and 1998 ESA and were provided by the Alaska SAR Facility.

References

Briole, P., D. Massonnet, and C. Delacourt, Post-eruptive deformation associated with the 1986–87 and 1989 lava flows of Etna detected by radar interferometry, *Geophys. Res. Lett.*, *24*, 37–40, 1997.

Byers, F. M., Geology of Umnak and Bogosl of Islands, Aleutian Islands, Alaska, *U.S. Geol. Surv. Bull.*, *1028-L*, 369 pp., 1959.

Dean, K., M. Servilla, A. Roach, B. Foster, and K. Engle, Satellite monitoring of remote volcanoes improves study efforts in Alaska, *Eos Trans. AGU, 79*(35), 413, 422–423, 1998.

Delaney, P. T., and D. F. McTigue, Volume of magma accumulation or withdrawal estimated from surface uplift or subsidence, with application to the 1960 collapse of Kilauea Volcano, *Bull. Volcanol.*, *56*, 417–424, 1994.

Delaney, P. T., R. S. Fiske, A. Miklius, A. T. Okamura, and M. K. Sako, Deep magma body beneath the summit and rift zones of Kilauea Volcano, Hawaii, *Science*, *247*, 1311–1316, 1990.

DeMets, C., R. G. Gordon, D. F. Argus, and S. Stein, Effect of recent revisions to the geomagnetic reversal time scale on estimate of current plate motions, *Geophys. Res. Lett.*, *21*, 2191–2194, 1994.

Lanari, R., P. Lundgren, and E. Sansosti, Dynamic deformation of Etna volcano observed by satellite radar interferometry, *Geophys. Res. Lett.*, *25*, 1541–1544, 1998.

Lu, Z., D. Mann, J. T. Freymueller, and D. J. Meyer, Synthetic aperture radar interferometry of Okmok volcano, Alaska: Radar observations, *J. Geophys. Res.*, *105*, 10,791–10,806, 2000.

Miller, T. P., R. G. McGimsey, D. H. Richter, J. R. Riehle, C. J. Nye, M. E. Yount, and J. A. Dumoulin, Catalog of the historically active volcanoes of Alaska, *U.S. Geol. Surv. Open File Rep., 98-582*, 1998.

Mogi, K., Relations between the eruptions of various volcanoes and the deformations of the ground surface around them, *Bull. Earthquake Res. Inst. Univ. Tokyo*, *36*, 99–134, 1958.

Nakamura, K., K. H. Jacob, and J. N. Davies, Volcanoes as possible indicators of tectonic stress orientation—Aleutians and Alaska, *Pure Appl. Geophys.*, *115*, 87–112, 1977.

Okada, Y., Surface deformation due to shear and tensile faults in a half-space, *Bull. Seismol. Soc. Am.*, *75*, 1135–1154, 1985.

Tait, S., C. Jaupart, and S. Vergniolle, Pressure, gas content and eruption periodicity of a shallow, crystallising magma chamber, *Earth Planet. Sci. Lett.*, *92*, 107–123, 1989.

Wicks, C., W. Thatcher, and D. Dzurisin, Migration of fluids beneath Yellownstone Caldera inferred from satellite radar interferometry, *Science*, *282*, 458–462, 1998.

J. Freymueller and D. Mann, Geophysical Institute, University of Alaska Fairbanks, P.O. Box 757320, AK 99775-7320, USA. (doerte@giseis.alaska.edu; jeff@giseis.alaska.edu)

Z. Lu, U.S. Geological Survey, EROS Data Center, Raytheon ITSS, Sioux Falls, SD 57198, USA. (lu@usgs.gov)

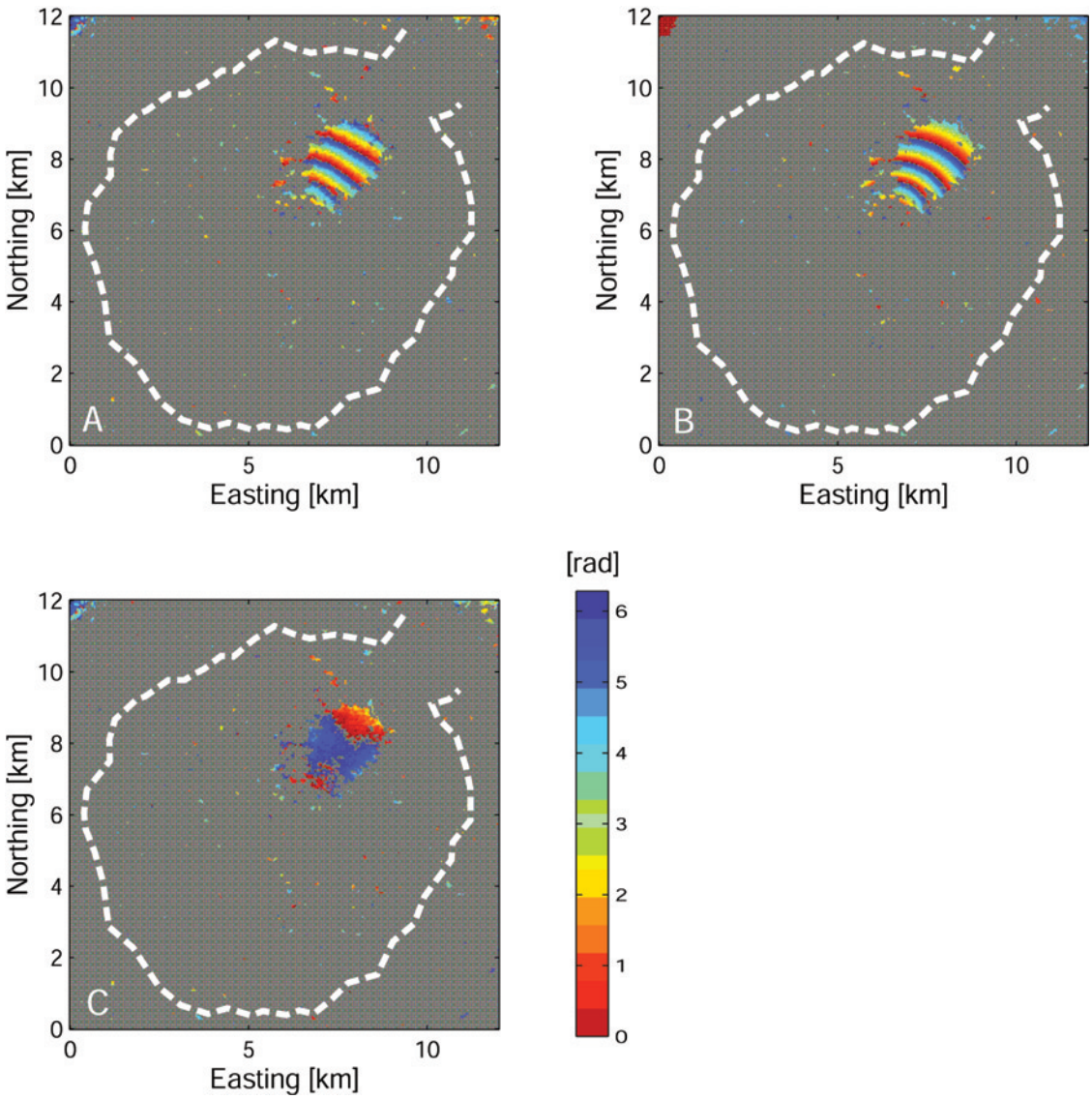

Figure 2. (a) Data, (b) best fit model, and (c) residual interferogram for the 1992–1993 preeruptive interferogram. The dashed line outlines the caldera. The origin of the coordinate systems is at 53.377°N, 168.220°W.

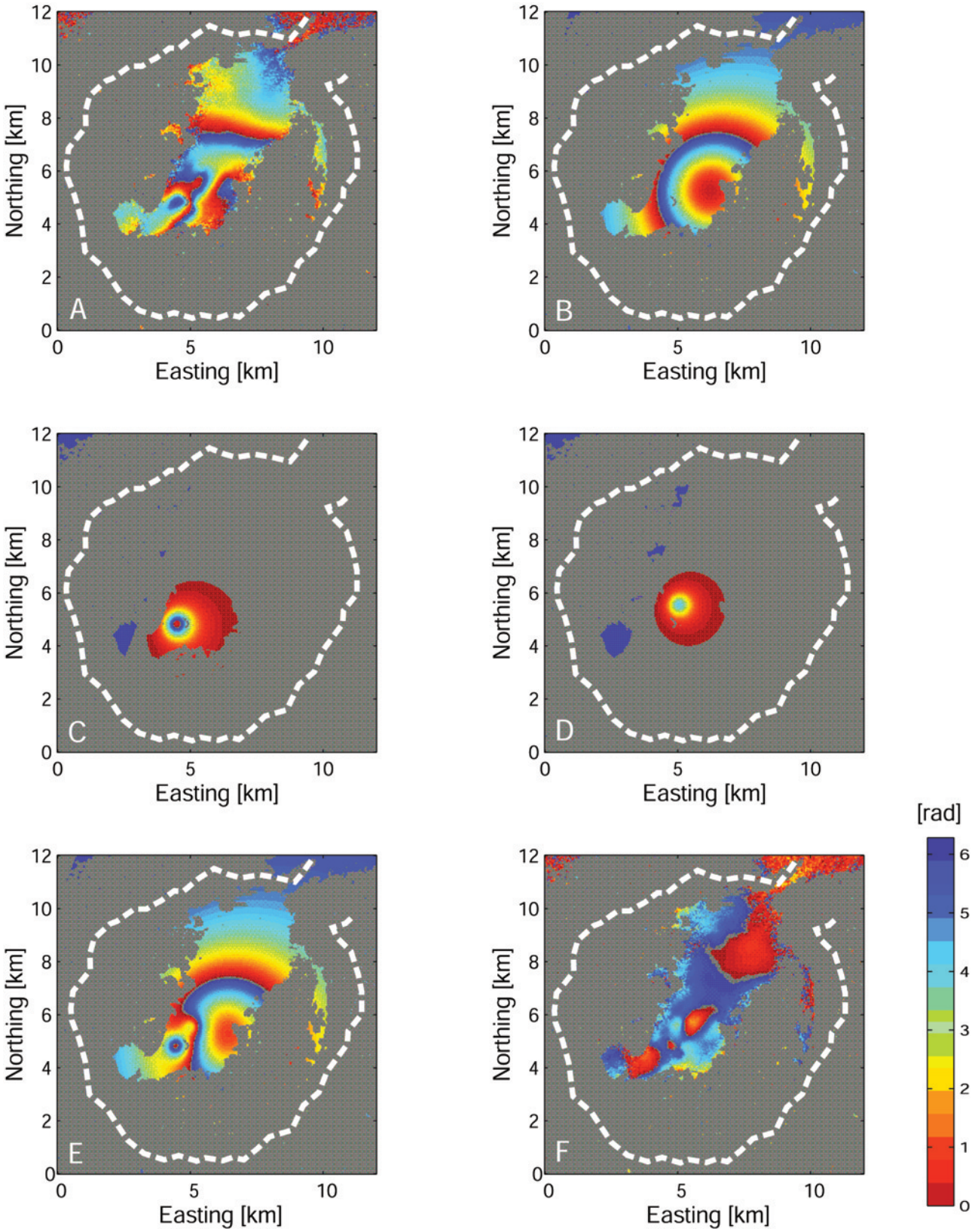

Figure 3. (a) Data, (e) best fit model, and (f) residual interferogram for the 1993–1995 preeruptive interferogram. (b, c, d) The model, consisting of three point sources with different depths and strengths. Annotations and origin of coordinate system are the same as in Figure 2.

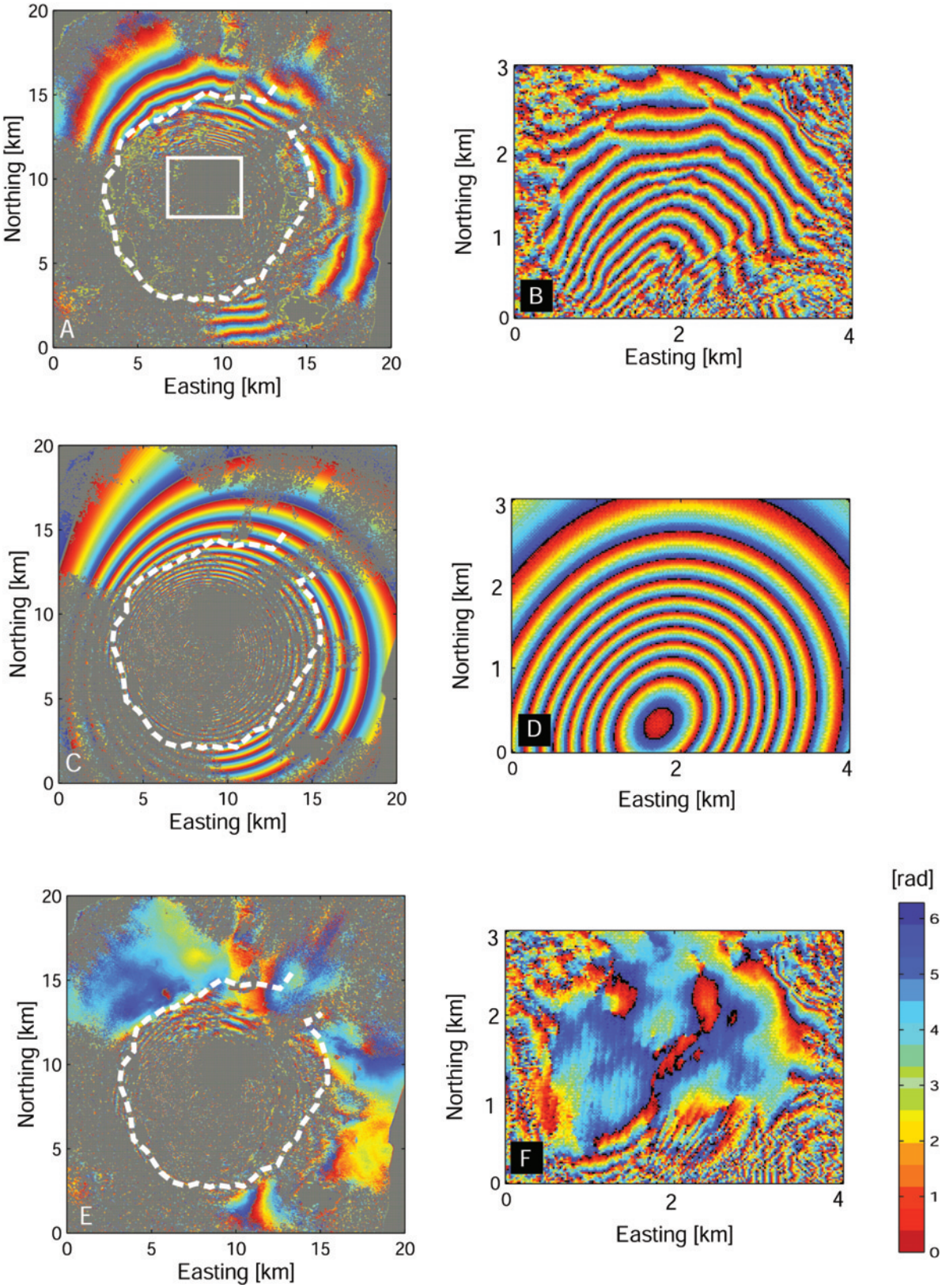

Figure 4. Data, models, and residuals for the 1995–1997 coeruptive interferogram. (a) Data of the 1995–1997 interferogram. The box outlines the area shown in Figures 4b, 4d, and 4f. The fringe density in the caldera center is too high to be properly displayed in Figure 4a. (b) Blowup of the data inside the caldera after subtracting the fringes explained by the best fit Mogi model for the outer part of the deformation shown in Figure 4c. (d) Best fit rectangular dislocation source for this data inside the caldera. (e) Residual interferogram for the combined modeling. (f) A blowup of the same residual interferogram, showing the model fit inside the caldera. The origin of the coordinate system for the large area is at 53.357°N, 168.257°W.

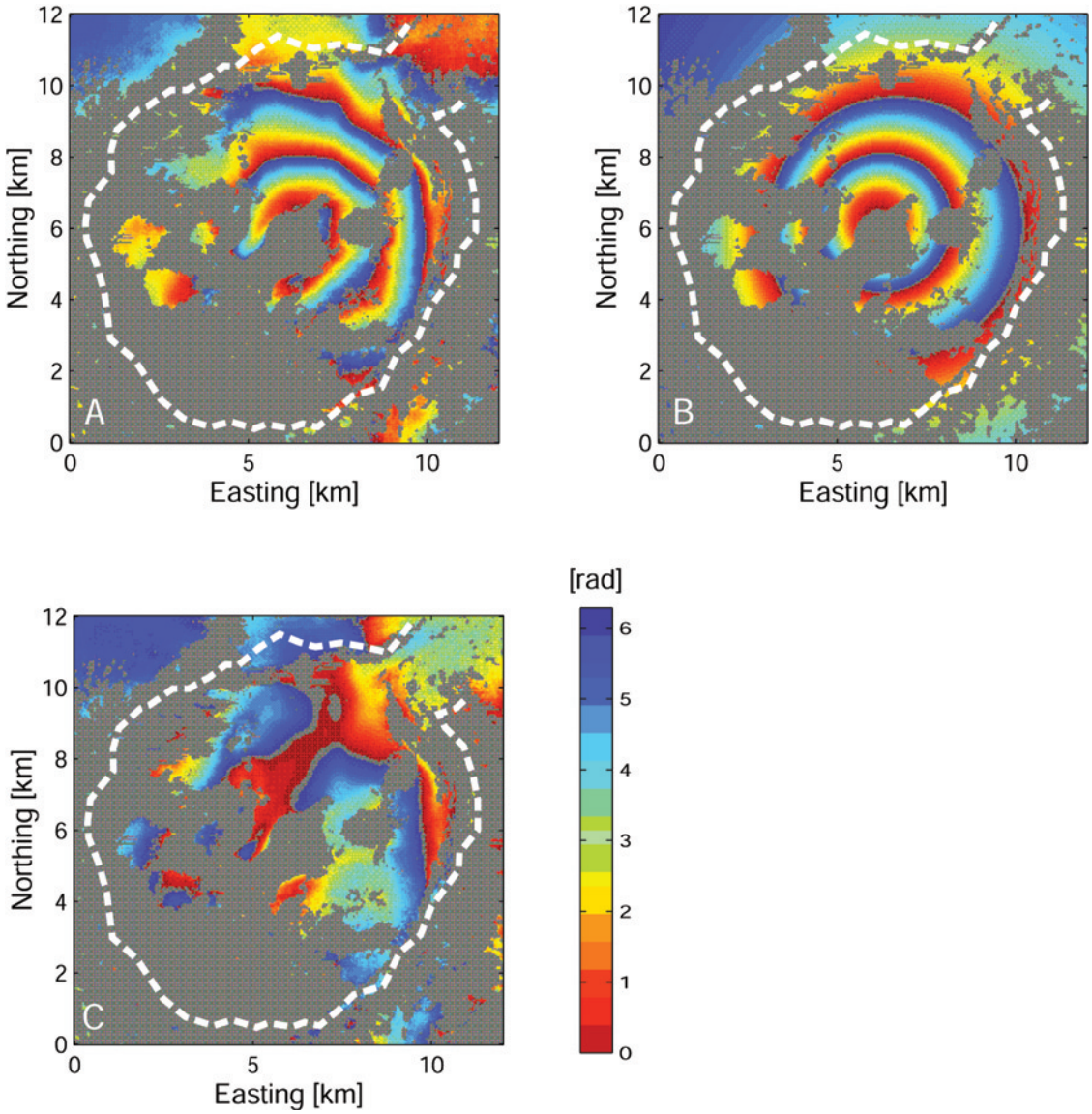

Figure 5. (a) Data, (b) best fit model, and (c) residual interferogram for the 1997–1998 posteruptive interferogram. Annotations and origin of coordinate system are the same as in Figure 2.

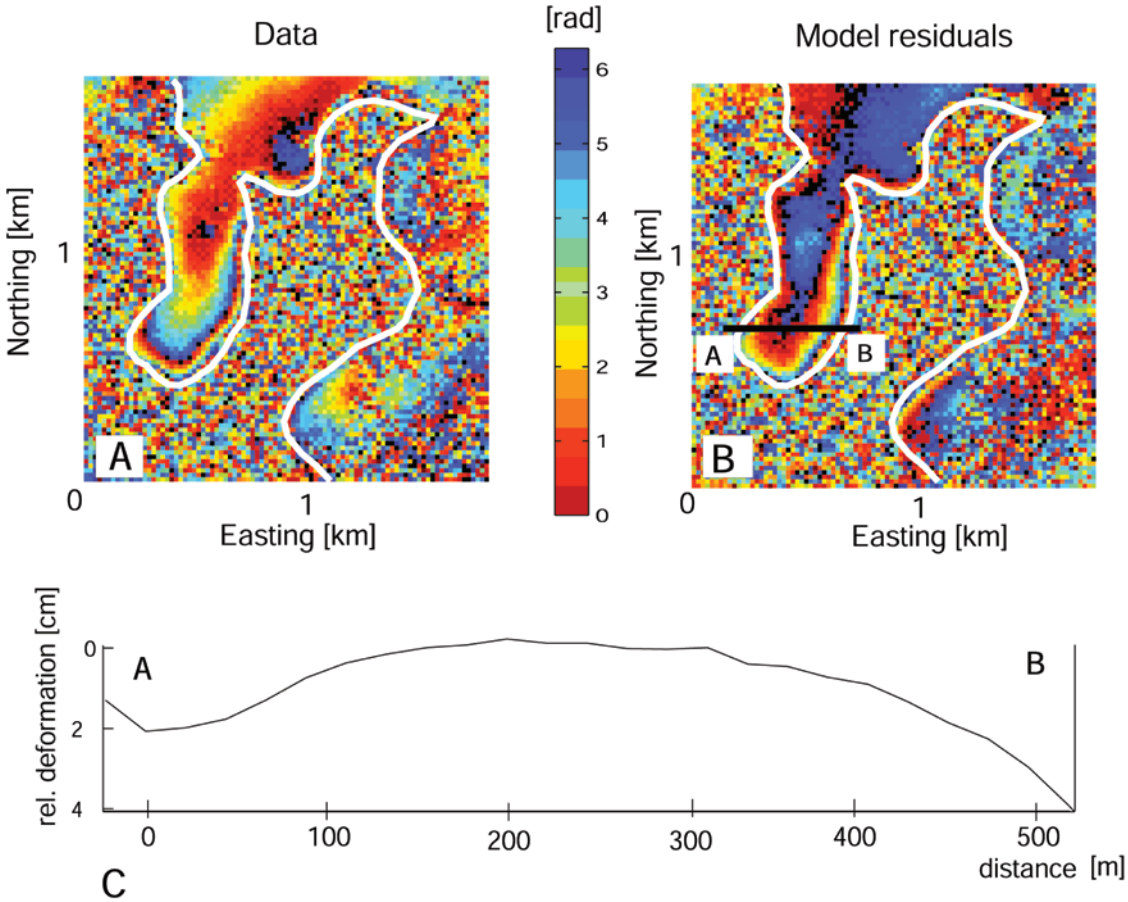

Figure 6. (a) Deformation fringes along the edges of the new lava flow as observed in the 1997–1998 interferogram. The white line outlines the flow boundary. (b) Residual fringes along the edge of the flow after subtracting the best fit Mogi inflation model from the data. The black line marks the profile shown in Figure 6c. (c) Deformation profile as marked in Figure 6b. Relative deformation across the profile is ~3 cm.